A comparison of inversion techniques for estimating Vp/Vs from 3D seismic data

Paul F. Anderson and Laurence R. Lines

ABSTRACT

There are a variety of methods that can be used to extract rock-properties information from seismic data. Three of the methods that can be used, include;

1. AVO analysis, followed by post-stack inversion of the AVO attributes (Goodway, et al.)

2. Prestack inversion of the P-wave data directly to impedance (Hampson et al.)

3. Joint prestack inversion of the P-wave data and converted wave data directly to impedance (Hampson et al.)

After each of these inversions has completed one of a variety of rock properties can be calculated. This paper compares the results of estimating Vp/Vs using each of the above mentioned techniques.

INTRODUCTION

Apache Canada Ltd. began an experiment with multicomponent seismic data in 2004 with an eastern Alberta 3D3C acquired with I/O Vectorseis MEMS geophones. The primary target in this experiment was, and continues to be, Mannville-age channel sands. The channel is easily identifiable on 3D seismic data, though reservoir quality issues remained an issue. It was hoped that the multicomponent seismic data would provide the leverage necessary to aid in drilling gas wells with a higher degree of success. In November 2006, Anderson and Larson showed that that hope appears to have been realized, with look-back success rates improving from 31% with P-wave seismic only, to 65% when integrating the information from the P-wave and converted wave volumes. A project was then undertaken to evaluate the differences in predicting rock properties, specifically Vp/Vs, from seismic data using one of three paths:

1. Amplitude variation with offset (AVO) analysis followed by post-stack inversion of the AVO attributes

2. Prestack inversion of the P-wave gathers directly to impedances

3. Joint prestack inversion of the P-wave gathers and a converted wave volume

The procedure and results from that analysis are presented below. A map of the seismic data identifying the relative positions of the wells is provided in Figure 1.

POST-STACK INVERSION METHOD

The process of estimating Vp/Vs with a post-stack inversion method follows the procedure outlined by Goodway et al. (1997). In this paper, the authors propose starting

with prestack data and performing an amplitude variation with offset (AVO) inversion of these gathers, in order to estimate the P-wave and S-wave impedances. One such method is the approximation to the Knott-Zoeppritz equations, proposed by Fatti et al. (1984), where AVO is estimated by performing a least-squares fit of the amplitudes from each time sample of the gather to an equation of the form:

$$R(\theta) \approx \tfrac{5}{8}\frac{\Delta V}{V} - \frac{W^2}{V^2}\left(4\frac{\Delta W}{W} + \tfrac{1}{2}\frac{\Delta V}{V}\right)\sin^2\theta + \tfrac{1}{2}\frac{\Delta V}{V}\tan^2\theta \qquad (1)$$

where, R(θ) is the reflectivity at any given angle (θ), P-wave Velocity Reflectivity, S-wave Velocity Reflectivity, Background Vs/Vp ratio.

The AVO inversion of prestack P-wave seismic gathers generates P-wave reflectivity and S-wave reflectivity. Using well log information, we can build background P-wave and S-wave impedance models which we can then be used to invert the corresponding AVO attributes for P-wave impedance and S-wave impedance following standard practices for acoustic impedance inversion. This workflow is described in Figure 2.

The gathers, as delivered by the processor, had additional processing applied in order to help improve the results. This consisted of a mute function applied to the data, as well as a 3x3 superbin, in order to improve the signal to noise ratio at each offset, through partial stacking (Ostrander, 1984). In order to convert from offset domain to angle domain for the CMP gathers, the stacking velocity was used to perform a 1-D pseudo-depth conversion, which when used with the offset of the traces within each CMP, produces the angle for each sample. A maximum angle of 30° was used for the AVO inversion, as farther angles begin to exhibit problems with normal move-out removal, either from inappropriate velocities, or non-hyperbolic move-out. AVO inversion used a background relationship between shear velocity and P-wave velocity given by Castagna's mud-rock line (Castagna, 1984);

$$Vs = -1172 + 0.862 * Vp \qquad (2)$$

Figure 3 shows an example of a characteristic offset gather with angles defined as the background colour. Upon extraction of the AVO attribute volumes, post-stack inversion was performed upon each attribute. Cross-sections taken from the P-wave and S-wave reflectivities are shown in Figure 4.

A single well log was used to build the impedance models. This well (Well E) contained measured conventional and shear sonic logs, in addition to density and other commonly acquired wire-line tools. We therefore have a direct measurement of the velocities for both P-waves and S-waves, in the vicinity of the borehole. Using the sonic logs available from four wells, time-depth relationships were created by manually aligning key events. A synthetic trace was created using the reflectivity derived from the sonic and density logs, convolved with a zero-phase statistical wavelet extracted from the seismic data Figure 5). The quality of the well log correlations was quite good, as shown in Figure 6 and because S-wave reflectivity is already in P-wave time, no additional correlations are necessary for the S-wave volume, however an independent wavelet (zero-

phase statistical) was used in the inversions, to better reflect the amplitude spectrum present on the S-wave reflectivity volume.

Using time-depth relationship for Well A, an impedance model was created to be used for the P-wave and S-wave inversions. Hampson-Russell software was used in all inversions. In the case of the post-stack inversion of the AVO attributes, a Model-Based inversion was performed. The inversion parameters are specified in table 1, and are consistent for both the P-wave and S-wave inversions.

Table 1. Post-stack inversion parameters

Prewhitening		1%
Scalar Adjustment Factor		1
Number of Iterations		10
Maximum Impedance Change		± 100%
Average Block Size		2 ms
Scaling Window	Top	200 ms above Base Fish Scales
	Base	50 ms below Rex Coal

After the inversions have been completed, calculation of the Vp/Vs is a simple matter of trace math given by;

$$V_p \Big/ V_s = \frac{Z_p}{Z_s} \tag{3}$$

Figure 7 is an example of the calculated Vp/Vs volume. The correlation of the Vp/Vs volume from post-stack inversion to well control will be discussed later, though it is worth mentioning at this point that the correlation appears to be quite good.

PRESTACK INVERSION WITH P-WAVE SEISMIC DATA

The procedure for prestack inversion of P-wave seismic data followed the workflow presented by Hampson et al. (2005). The concept is intended to arrive at the same point as the workflow provided above, using fewer steps and in a more integrated fashion. One of the less favorable aspects to the post-stack inversion method described above is the inversions for P-Impedance and S-Impedance, with the exception of the models, are independent of one another. Non-correlated noise can cause problems because the signal to noise ratio of the P-wave reflectivity and S-wave reflectivity are different, the resulting inversion can respond to this in different ways on each section. By performing the inversion prestack, we are able to solve for P-wave impedance and S-wave impedance simultaneously, thereby treating errors equally on both volumes.

The same gathers used for the AVO extraction above were used as a starting point for the prestack inversion. Using the stacking velocities, the offset gathers were converted to angle gathers (Figure 8), using seven angles between 0° and 35°. For the inversion, however, only angles between 5° and 30° were used, due to acquisition footprint issues (near offsets) and periodic NMO-correction errors (far offsets).

In order to maintain consistency, the background model used for the post-stack inversions was also used for the prestack inversion. Because the algorithm is somewhat different, parameterization is not the same as in the case of the prestack inversion, as we are optimizing the inversion for seven prestack traces at each CMP location, instead of one post-stack trace. To do so, the prestack inversion requires a background trend between P-wave impedance and S-wave impedance, as well as P-wave impedance and density. The inversion then solves the angle-dependant reflectivity model that minimizes the error on the angle gathers as deviations from the input model. These deviations from the model are then added back to the model and the process is repeated, generally with significantly more iterations than typically done with a post-stack inversion to reach what is hoped to be a global minimum. Using the model built from Well A and the background relationships between P-Impedance, S-Impedance and Density from four wells (Wells A, C, D andE), the prestack inversion parameters used are defined in table 2 guided by the cross-plots shown in Figure 9.

Table 2. Prestack inversion parameters.

Angles Used		5 - 35
Number if Iterations		50
Joint k (from figure 9)		1.050752
Joint kc (from figure 9)		-5.30515
Joint m (from figure 9)		0.025122
Joint mc (from figure 9)		-0.934635
Prewhitening	P-Impedance	25%
	S-Impedance	25%
	Density	100%
Scalar Adjustment Factor		1
Scaling Window	Top	75 ms above Base Fish Scales
	Base	50 ms below Rex Coal

In order to account for frequency content differences from near to far angles, near angle (5°) and far angle (25°) wavelets were extracted using the same parameters as the wavelets derived from the post-stack inversion. This allows the wavelet to account for frequency dependant changes in the angle gathers that are not attributable to geology (frequency decay with offset, wavelet stretch from NMO-removal – Figure 10, etc.). The resulting wavelets are shown in Figure 11. In this case, a full-phase wavelet was extracted using the Roy-White algorithm within HRS-STRATA software to account for phase variations with offset that we can see are present in this data as the difference in the "average phase" (the intercept of a line fit through the phase versus frequency over the signal band of the wavelet) is 28°. A profile from the resulting Vp/Vs volume is shown in Figure 12. Inserting the Vp/Vs log from the wells, the correlation is quite good over the zone of interest, with the possible exception of the coal layers immediately above the target sand. This may be due to a violated assumption in the AVO inversion, which will be discussed later.

PRESTACK INVERSION WITH P-WAVE AND CONVERTED WAVE SEISMIC DATA

Integration of the converted wave data to the inversion follows a similar path as previously defined for the PP-only prestack inversion. Using the same P-wave angle gathers created for the previous inversion, we also include input from the converted wave data. However before incorporating the converted wave information, we must first ensure that all data to be used is in a common time domain. The issue is that conventional (P-wave) seismic data is recorded in time, however this is really the time for a P-wave to travel a specified distance. In the case of NMO-corrected P-wave data, this is the T_0 time given by the move-out equation and is defined by;

$$T_0 = \frac{2z}{V_{P-ave}} \tag{4}$$

where $V_{P\text{-}ave}$ is the average P-wave velocity for a source wavelet to travel from the surface, to the reflector and back again at zero offset. In the case of converted waves however, this equation must be modified such that we account for the wave traveling down at P-wave velocity and returning at S-wave velocity;

$$T_0 = z\left[\frac{1}{V_{P-ave}} + \frac{1}{V_{S-ave}}\right] \tag{5}$$

where the reflected S-wave returns at a velocity $V_{S\text{-}ave}$. This however, leads to a difficulty, specifically that we do not explicitly know the S-wave velocity to each event in our seismic section, in much the same way we do not know P-wave velocities well enough to do perfect depth conversions.

The solution is to correlate events of key geologic markers that are regionally consistent and visible on both the P-wave and converted wave seismic sections. Because we have correlated well logs to P-wave seismic sections, we know where each geologically significant event exists on P-wave gathers, which we can repeat with the converted wave data. Using the correlated P-wave sonic log and the integrated S-wave sonic log, the software can develop a converted wave synthetic. We can now correlate the converted wave synthetic to the converted wave seismic data following the same procedure used previously for the P-wave data. Given the resulting depth to converted wave time relationship, we can now identify which geologic events are consistent between the P-wave and converted wave volumes (Figure 13).

We now have two methods of calculating the Vp/Vs from the well log data;

1. ratio of the compressional and shear sonic logs
2. ratio the depth-time curves derived by correlating synthetics to the P-wave and converted wave volumes.

Differences between these may exist due to a variety of factors, including attenuation effects, however they are expected to be relatively consistent with one another. These

curves will be compared in a later section. Now that we have the ability to register the data at the wells, we need to extend that throughout the volume. To do that we used the previously mentioned geologic markers that are consistent between the p-wave and converted wave sections. First we pick these horizons throughout each volume independently. Once that is completed, we can now force the converted wave horizons to P-wave time. To do this we go back to the equations defined above for zero-offset travel times. Given that we do not know the depth of the reflectors, we can rearrange the equations solving for depth (z) and equate them;

$$T_p = \frac{2z}{V_{P-ave}},\ T_{ps} = z\left[\frac{1}{V_{P-ave}} + \frac{1}{V_{S-ave}}\right] \tag{6}$$

$$\frac{T_p V_p}{2} = z,\ z = \frac{T_{ps}}{\left[\frac{1}{V_{P-ave}} + \frac{1}{V_{S-ave}}\right]} \tag{7}$$

$$\frac{T_p V_p}{2} = \frac{T_{ps}}{\left[\frac{1}{V_{P-ave}} + \frac{1}{V_{S-ave}}\right]} \tag{8}$$

$$\frac{V_p}{V_s} = 2\frac{T_{ps}}{T_p} - 1 \tag{9}$$

However, because when processing converted wave data we are unable to exactly ensure that it is using the same datum as our P-wave volume, we reformulate equation 8 to;

$$\frac{V_p}{V_s} = 2\frac{\Delta T_{ps}}{\Delta T_p} - 1 \tag{10}$$

where the Vp/Vs calculated is valid for the time window over which the isochrons are calculated. Because of the datum issue mentioned above, the first layer accounts not only for the Vp/Vs of the layer, but also for the differences in datuming, so is therefore assumed to be non-geologic and is only used for registration purposes. When performing the registration in this manner, it is important to watch that the domain-specific reflectivities are accounted for. For example, it is possible that an event used for horizon based registration is a peak on the P-wave volume (i.e. an impedance increase) but is a trough, zero-crossing or something in between on the converted wave volume. Errors of this nature will result in registration errors and could result in non-geologic Vp/Vs being calculated, as such it is important to ensure that the Vp/Vs derived from the horizon based technique is consistent with well control. Figure 14 shows the converted wave data in P-wave time with the background colour defined as the layer based Vp/Vs. The Vp/Vs calculated from the depth-time curves has been inserted into the section for comparison, in this case it appears to be a fair match. While we are able to use this Vp/Vs to register the volume to P-wave time, it is worth noting that it has considerably less resolution (i.e. detail) than is present in the background velocity model used for inversion (Figure 15). The geologic horizons used to build the registration Vp/Vs included the Base Fish Scales

(BFS), and the Rex Coal. Attempts were made to use additional horizons, however the differing frequency content of the volumes limits our ability to pick the same geologic event in order to produce geologically realistic Vp/Vs.

The resolution of this registration Vp/Vs is often too low to be of value in determining the rock properties of potential reservoir formations, unless the thickness of the layer used for registration is on a similar order of magnitude as that of the reservoir, as, because the velocities used in equation 9 are average velocities, the Vp/Vs are average ratios over each interval. As an aside, while not incorporated into the software at this time, there could be additional value in incorporating this registration Vp/Vs volume as a soft-constraint into the inversion. At this time, it is only used to register the converted wave data to P-wave time.

Now that we have the necessary information to register the converted wave data to P-wave time, we can now build the background model. This background model is the same as the model built in the previous prestack inversion, however it also incorporates the Vp/Vs from registration so as to register the converted wave data as part of the inversion process. Wavelets also need to be defined for use in the inversion and for the P-wave data, we are again using the near and far angle wavelets, however it is necessary to derive a wavelet from the converted wave data. This wavelet is derived from in the p-wave time domain over the same geologic intervals used for the p-wave wavelets. We can see in Figure 16 that the frequency content of the converted wave data, even after registration, is significantly lower than that of either of the P-wave wavelets. Because the wavelets in the inversion program are defined at specific angles, but we are using a full-offset stack for the converted wave data, we must choose an angle at which to define the converted wave data and the corresponding wavelet. In this case we chose an angle of 15°. Because low angles produce low converted wave reflectivities (PS reflectivity at zero offset is zero), and the far offsets are muted, the dominant portion of the data will follow a corridor through the prestack gather and the volume will have an average angle close to 15°. This is analogous to weighted stacking for AVO analysis as proposed by Gidlow and Smith (1992). Small errors in the estimation of this angle can be accounted for in the inversion itself when calculating the scalar to apply to the converted wave data, provided that the dominant angle of the converted wave data does not change with respect to time.

The inversion parameters are then selected and the inversion is rerun. Because the P-wave data consists of multiple traces, but the converted wave data is one trace, the inversion equations bias the P-wave data, unless the converted wave data is weighted higher (Hirsche). As such, inversions were tested with weights of 1.0 and 2.0, with a final selection of a weight of 1.0 being used for the full inversion as it appeared to suffer the least from the low-frequency content of the converted wave data. A cross-section of the Vp/Vs calculated via joint simultaneous prestack inversion is shown in Figure 17, with the Vp/Vs from the time-depth relationship inserted for comparison.

DISCUSSION

Figure 18 shows a comparison of the three different Vp/Vs methods for the same cross-line. Inserted into each section is the Vp/Vs calculated from depth-time relationships for comparison. One comment that can be made immediately is that each of

these volumes has different frequency content. The amplitude spectra of these Vp/Vs are displayed in Figure 19. Given that the seismic data all possessed the same filters (with the exception of the converted wave data) it is interesting to note the differences in the spectra. Comparing the wavelets, (Near versus Rp and Far versus Rs), we note some differences, particularly at the high frequencies on the Rs wavelet (Figure 20). It would appear that the weighted stacking process of AVO has preserved more high-frequency energy than is present on the individual angle stacks. This high-frequency content could be representative of real geology that has been preserved by stacking, or it is a result of noise contaminating the AVO attributes, and then into the inversion result. Based upon the inversion Vp/Vs, the high frequency content does appear to be noise. Interestingly, by going back one step to look at the amplitude spectra on the impedance volumes, the high frequencies on these attributes are much more suppressed (Figure 21). It is possible that we have accidentally demonstrated one of the potential pitfalls with the post-stack inversion technique. That pitfall is that while the inversion is running it is minimizing the error on the reflectivity estimates by iteratively changing the reflectivity of each sample. Since the inversion for P-Impedance and S-Impedance are decoupled, we may have a situation where the P-wave inversion may put a reflector at sample x, but that same geologic event may occur on the S-wave inversion at sample x-1 or x+1. When we then ratio these to attributes that effectively have a registration error, we produce high, frequency artifacts.

Examining the amplitude spectrum of the joint prestack inversion, we can see that using a cutoff of approximately 30 dB-down, that there appears to be a large number of "holes" in the resulting amplitude spectrum (Figure 19c). These holes occur where the amplitude spectra of the P-wave and converted wave data overlap in the frequency domain (Figure 16), from roughly 10 Hz to 50 Hz. One possible explanation is that there are errors present in the converted wave registration such that the geology on each volume effectively does not align, causing the inversion to solve for two different lithologies at the same time, which it cannot do except at certain frequencies where tuning or some other effect allows for a solution to exist, though this solution may still be non-geologic. The frequencies above the converted wave band (i.e. > 50 Hz) are unaffected as the only data contributing to a solution at those frequencies is the P-wave data. Further work on registration may help to improve these results.

Another possible explanation, however, is that the registration process has made the wavelet on the registered converted wave data non-stationary in time (and possibly space). This result comes from different portions of each converted wave trace being compressed a different amount, depending upon the Vp/Vs used for registration. This non-stationary wavelet violates one of the assumptions of the inversion program and as a result, the amplitude spectrum of the inverted result is corrupted within this frequency range. It is the author's intent to investigate this further in future research efforts.

Overall, the prestack inversion using P-wave data only appears to be a good compromise between the high frequency noise of the post-stack inversion and the relatively low frequency result using the joint prestack inversion.

While looking at the data at these scales, we could choose the prestack inversion using PP-data only as it appears to give the most laterally continuous inversion result that

appears to tie well to wells, but is it actually any better when we examine it in detail? One way to determine this is to plot the inverted results at the well locations over the Vp/Vs from well logs. Figure 22 shows the Vp/Vs from four well locations. Each well log track can be identified by:

Track 1: Density (blue), SP (black), Gamma-Ray (red)

Track 2: Vp/Vs from depth-time (filtered, blue), Vp/Vs from post-stack inversion (red), Vp/Vs from logs (filtered, black)

Track 3: Vp/Vs from depth-time (filtered, blue), Vp/Vs from prestack inversion (red), Vp/Vs from logs (filtered, black)

Track 4: Vp/Vs from depth-time (filtered, blue), Vp/Vs from joint prestack inversion (red), Vp/Vs from logs (filtered, black)

Track 5: Vp/Vs post-stack inversion (red), Vp/Vs from prestack inversion (black), Vp/Vs from joint prestack inversion (blue)

Overall, all three curves match relatively well to the measured response in the well, with the exception in all cases of around the coals. The limitation here comes from the assumption in the Aki and Richards (1980) approximation to the Knott-Zoeppritz equations, where it is assumed that reflectivity contrasts are relatively small (i.e.). This is true of all three inversion methods mentioned above. Because the reflectivity contrast of the coals is so high, approaching 10 times higher than the average background reflectivity (Figure 23), this assumption is violated and the solution at that level is therefore left in doubt.

CONCLUSIONS AND FUTURE WORK

In summary, three different inversion methods were tested and evaluated based upon their ability to estimate Vp/Vs from well logs data.

1. Amplitude variation with offset (AVO) with two post-stack inversions
2. Prestack inversion of P-wave data only
3. Joint-prestack inversion of P-wave and converted wave data

Based upon the results presented here, prestack inversion alone appears to be the best method to estimate Vp/Vs from seismic data, however, future work could impact these results. Specifically, reprocessing the converted wave data so as to account for shear wave birefringence may significantly improve the amplitude correlation as well as the frequency content of the converted wave data, which could improve accuracy of both the registration and the joint prestack inversion. Additionally, more detailed registration work may better align geology between the P-wave and converted wave volumes, resulting in better joint inversions.

Incorporation of the Vp/Vs from registration as part of the background model, perhaps as a soft constraint, could improve all three inversion techniques. Revised processing of the P-wave data to incorporate farther offsets/angles may help to constrain the inversion results, perhaps even allowing an inversion for density. This would require higher-order move-out corrections or other brute-force methods to implement (e.g. time-variant trim static).

It has been noted that the AVO plus post-stack inversion flow has potential pitfalls, which appear to have been encountered with this data set, due to the fact that we are solving for related parameters in an unrelated fashion, which has resulted in artifacts (high-frequency noise on subsequent products like Vp/Vs). Registration of the converted wave data violates the "stationary wavelet" assumption inherent in the inversion process. Additional research is needed, however, in order to find a method to resolve this issue. Caution should be exercised when estimating rock properties from seismic data that contains geology which violates any of the assumptions used in the rock properties extraction.

Based upon the results shown to date, the prestack (P-wave only) inversion appears to have produced the best correlation to well control with a relatively small amount of noise generated as a result of the inversion process.

ACKNOWLEDGEMENTS

Special thanks to the staff at Apache Corporation for providing the data and encouragement to continue pushing this data volume to its limits, specifically to David Monk, Ron Larson and Heather Joy. Also to CGGVeritas Hampson-Russell for software support and extensive code debugging for the joint prestack inversion presented above, especially to Janusz Peron, Keith Hirsche and Graham Carter. Thanks also go to VGS Seismic for providing publication rights on the P-wave seismic data. Most especially, thank you to my wife and kids for their love, encouragement and support throughout my return to the school environment. We also acknowledge the sponsors of CREWES for their support.

REFERENCES

Aki, K. and Richards P.G., 1980, Quantitative Seismology, v. **1**, sec 5.2

Anderson, P. F., and R. Larson, 2006, Multicomponent case study - One company's experience in Eastern Alberta: Recorder, **31**, 5–10.

Fatti, J.L., Smith, G.C., Vail, P.J., Strauss, P.J., and Levitt, P.R. 1994, Detection of gas in sandstone reservoirs using AVO analysis: A 3-D seismic case history using the Geostack technique. Geophysics, **59**, 1362-1376.

Gidlow, P. M., Smith, G. C., and Vail, P. J., 1992, Hydrocarbon detection using fluid factor traces, a case study: How useful is AVO analysis? Joint SEG/EAEG summer research workshop, Technical Program and Abstracts, 78-89.

Goodway, B., Chen, T. and Downton, J., 1997, Improved AVO fluid detection and lithology discrimination using Lame petrophysical parameters; 'λρ', 'μρ', and 'λ/μ fluid stack' from P and S inversions, 67th Ann. Internat. Mtg: Soc. of Expl. Geophys., 183-186.

Hampson, D. P., B. H. Russell, and B. Bankhead, 2005, Simultaneous inversion of pre-stack seismic data: 75th Annual International Meeting, SEG, Expanded Abstracts , 1633-1637.

Hirsche, K., 2003 – 2008, Personal communication.

Ostrander, W. J., 1984, Plane-wave reflection coefficients for gas sands at nonnormal angles-of-incidence: Geophysics, **49** , no.10, 1637-1648

FIGURES

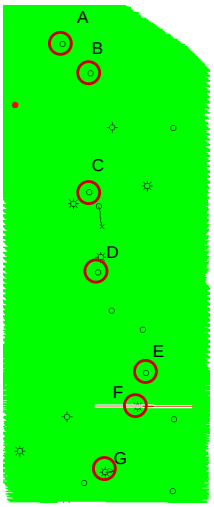

FIG. 1: Map of portion of 3C3D volume with wells identified. Wells A, C, D and E have dipole sonic log measurements and Well F has a Vp/Vs log derived from a 3C-VSP experiment

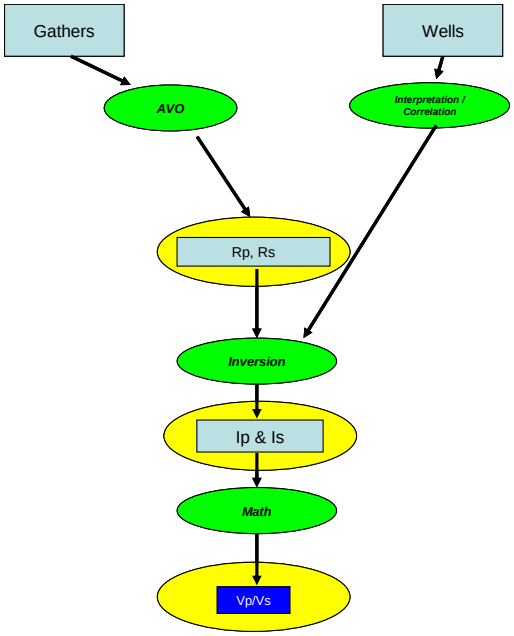

FIG. 2: Workflow for calculating Vp/Vs volume from seismic data using AVO and post-stack inversion

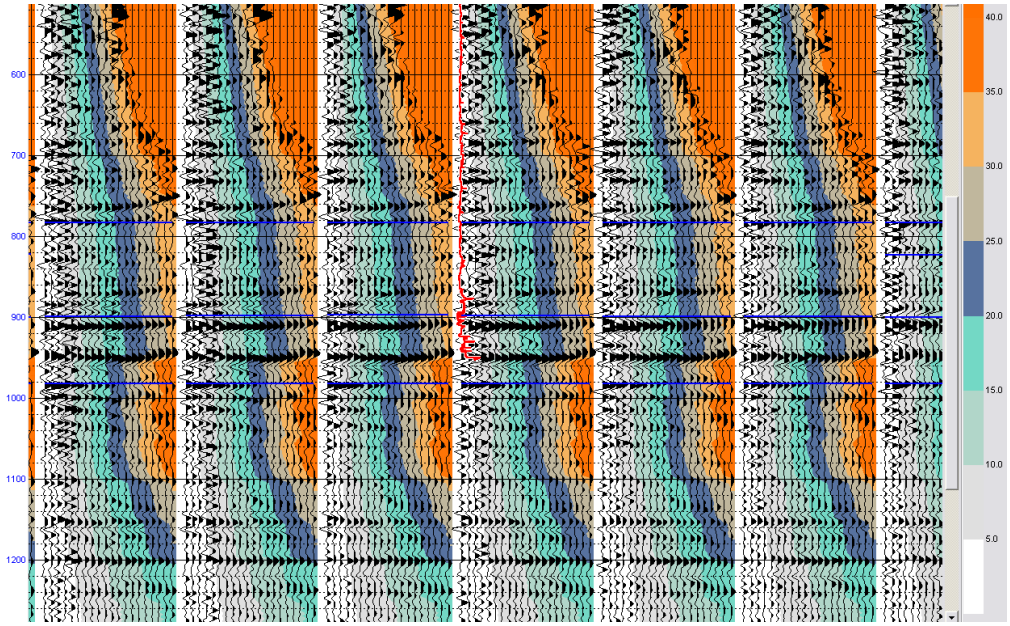

FIG. 3: Prestack P-wave seismic data. Angles are displayed as colour background. Target zone has a maximum angle slightly above 30°

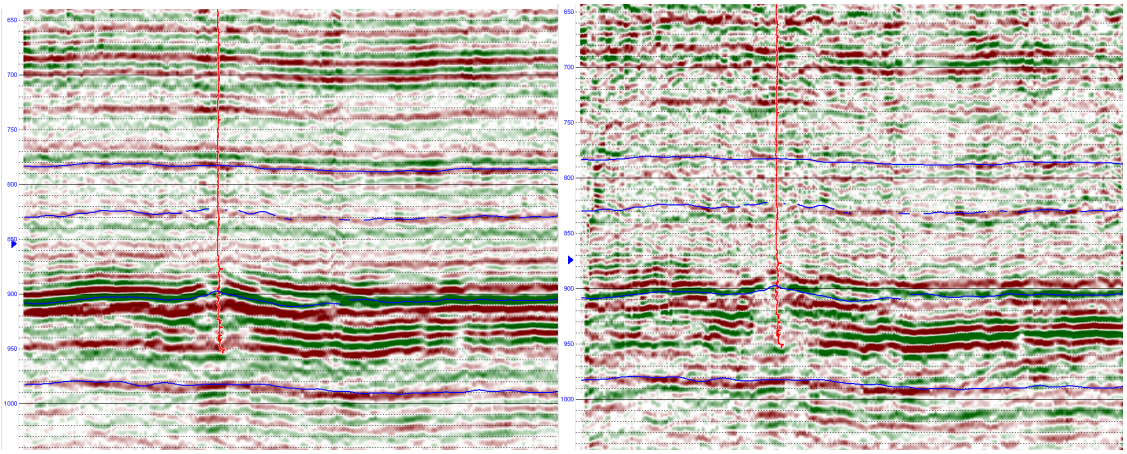

FIG. 4: AVO attributes Rp (left) and Rs (right). The sonic log from Well F is shown as the red trace in the displays. The zone of interest is at approximately 925 ms.

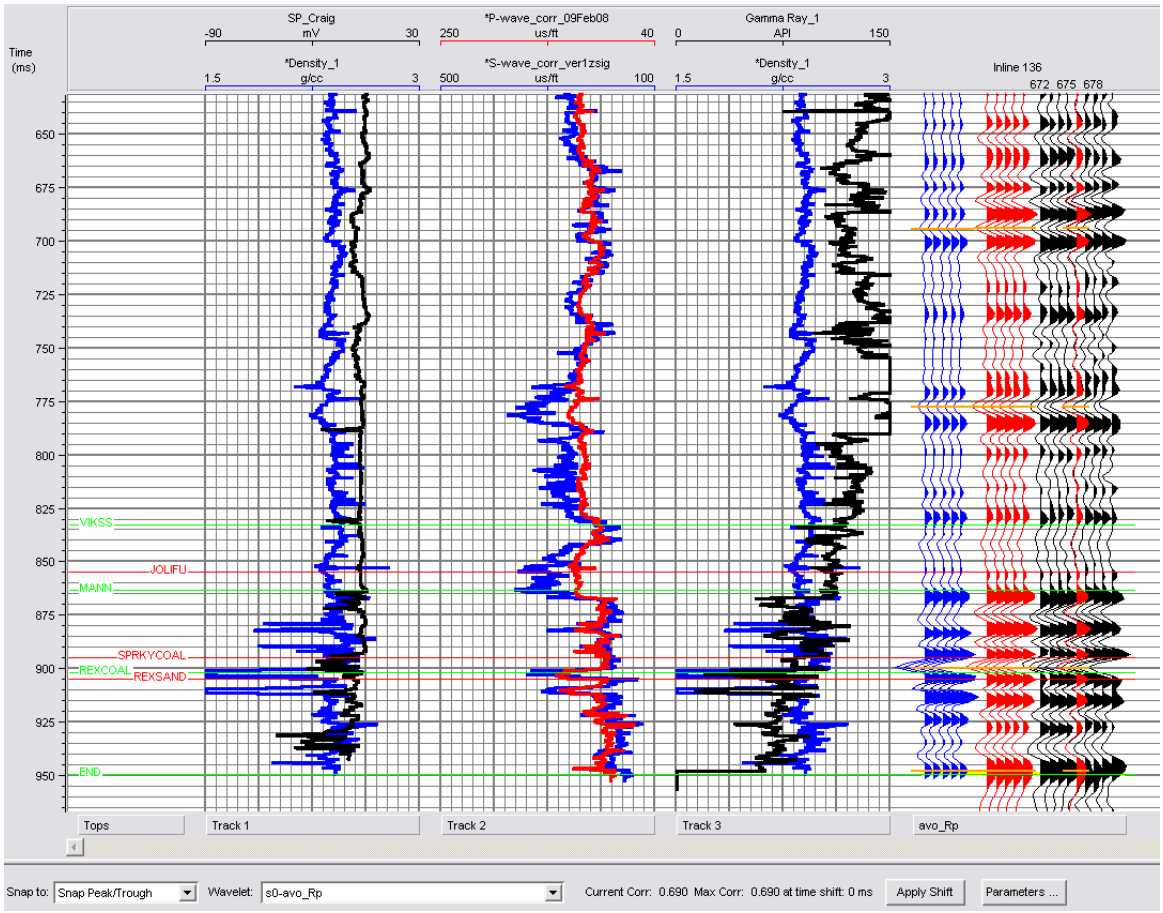

FIG. 5: P-wave synthetic to seismic well tie for well D. The blue wiggle trace is the synthetic and the red wiggle trace is the seismic data at the well location. Correlation is 69%.

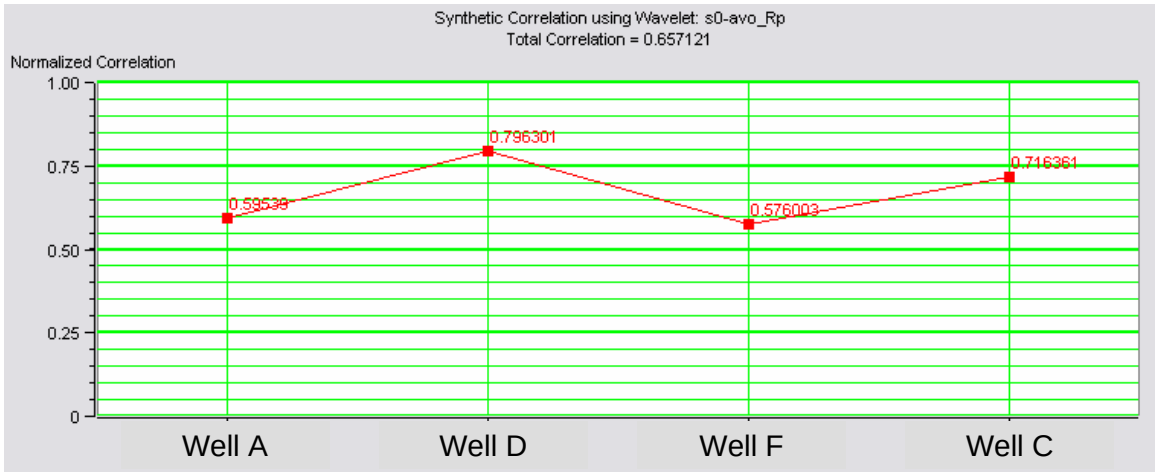

FIG. 6: P-wave synthetic correlations to seismic data at four wells, indicating reasonable quality well ties.

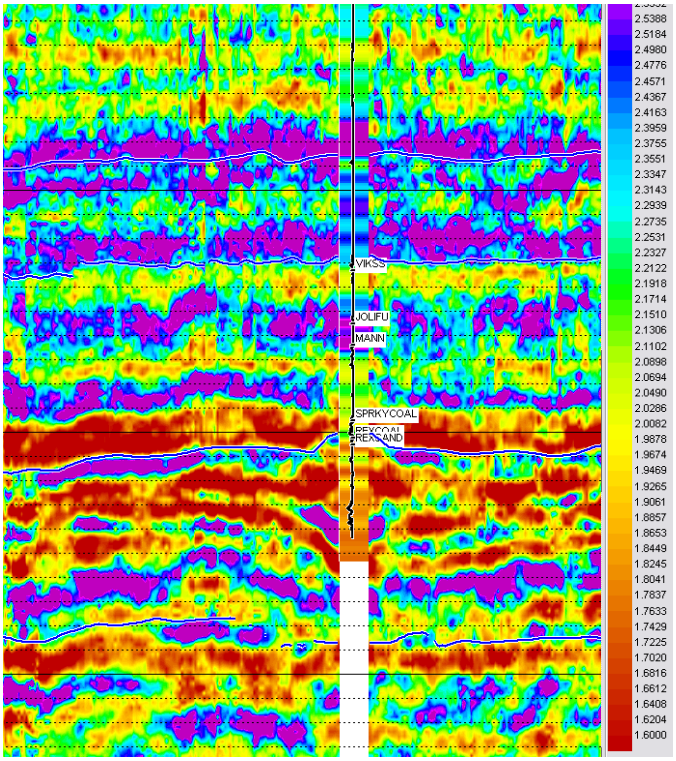

FIG. 7: Vp/Vs from AVO and post-stack inversion. Vp/Vs from logs at Well D has been inserted in colour and the SP log as the trace.

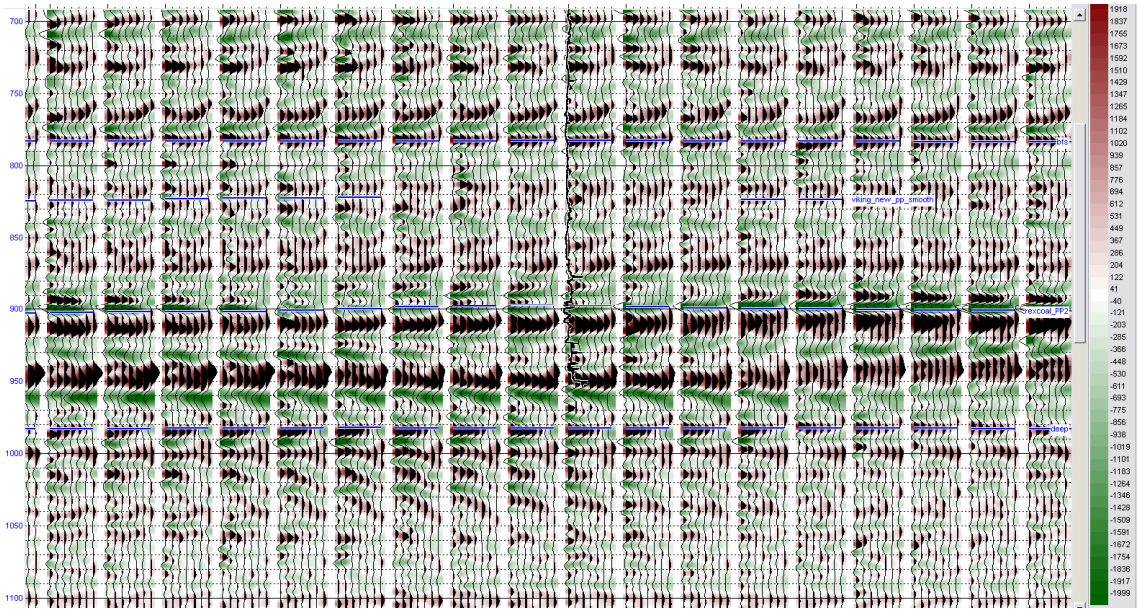

FIG. 8: 7-fold (0°-35°) angle gathers from around Well F.

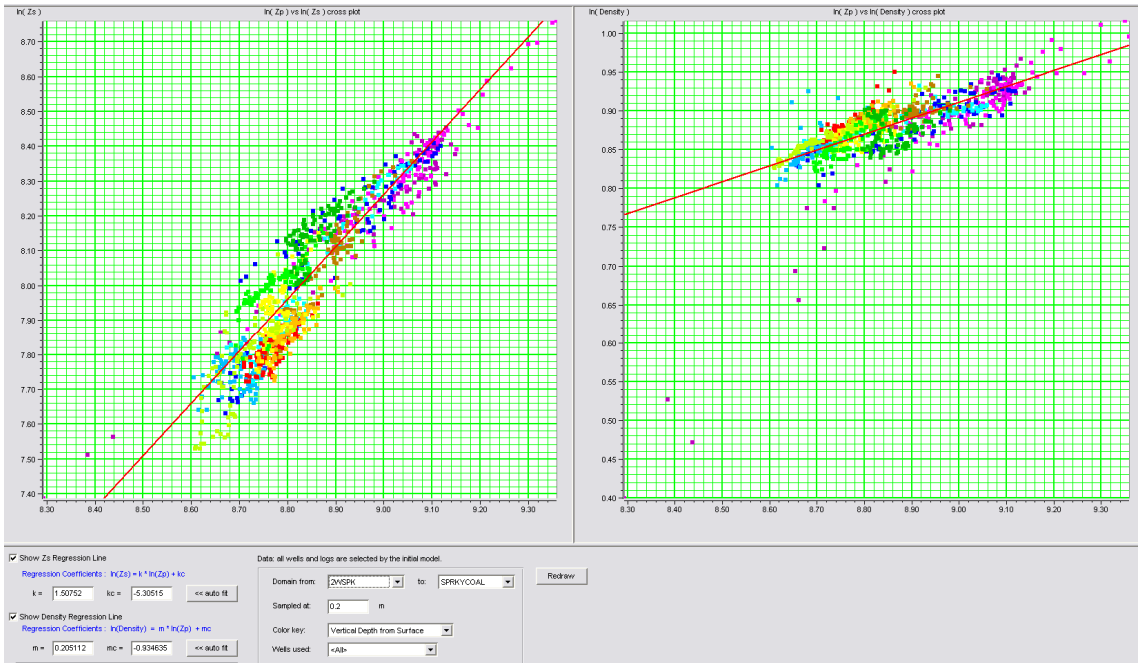

FIG. 9: Display of prestack parameterization menu. Left image is a cross-plot of the natural log of P-Impedance versus the natural log of S-Impedance. The right image is a similar plot of the natural log of P-Impedance versus the natural log of density.

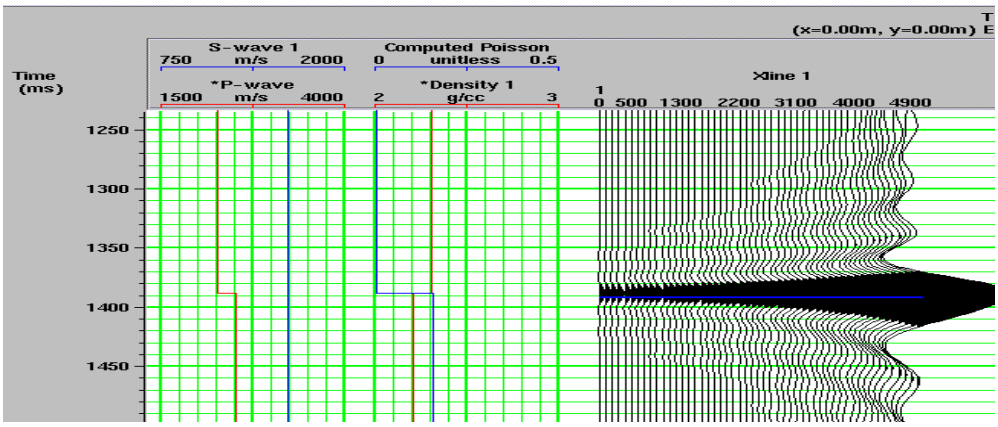

FIG. 10: Simple 1-layer model showing the exaggerated effect of NMO-stretch on a simple reflector. Note that the same wavelet was used to generate the wavelet at all offsets before NMO-removal.

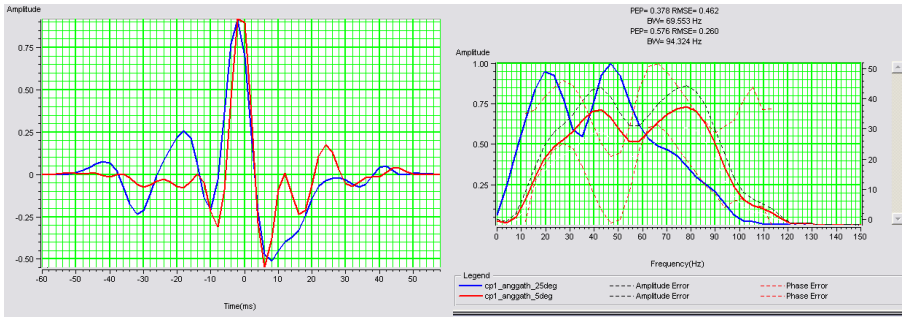

FIG. 11: Near (blue) and far (red) angle wavelets used in prestack inversion. In addition to differing frequency content, the average phase of the wavelet is 26° for the near angle and 54° for the far angle.

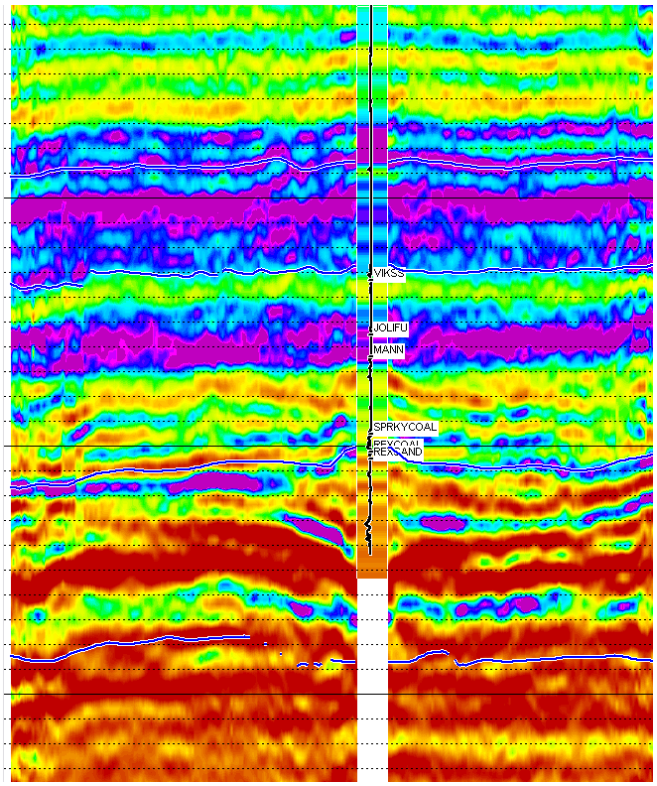

FIG. 12: Vp/Vs from prestack inversion. Vp/Vs from logs at Well D has been inserted in colour and the SP log as the trace.

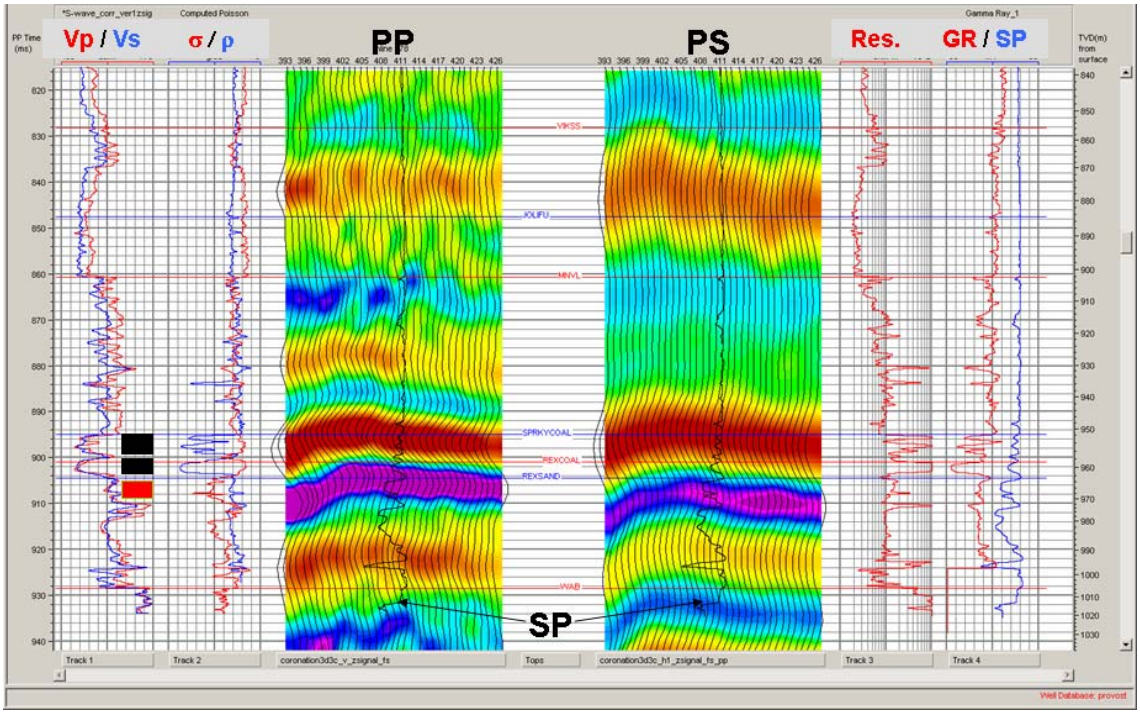

FIG. 13: Correlation of logs to P-wave data and to converted wave data allows identification of hey horizons in both domains.

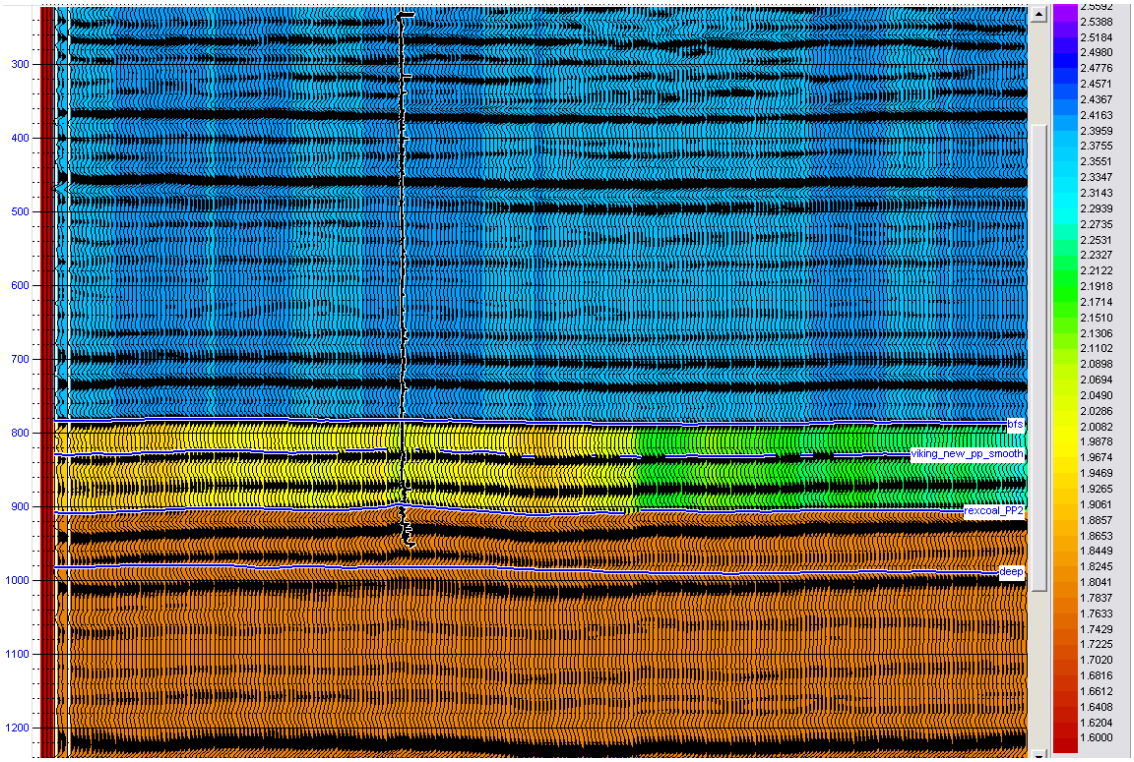

FIG. 14: Vp/Vs from horizon-based registration.

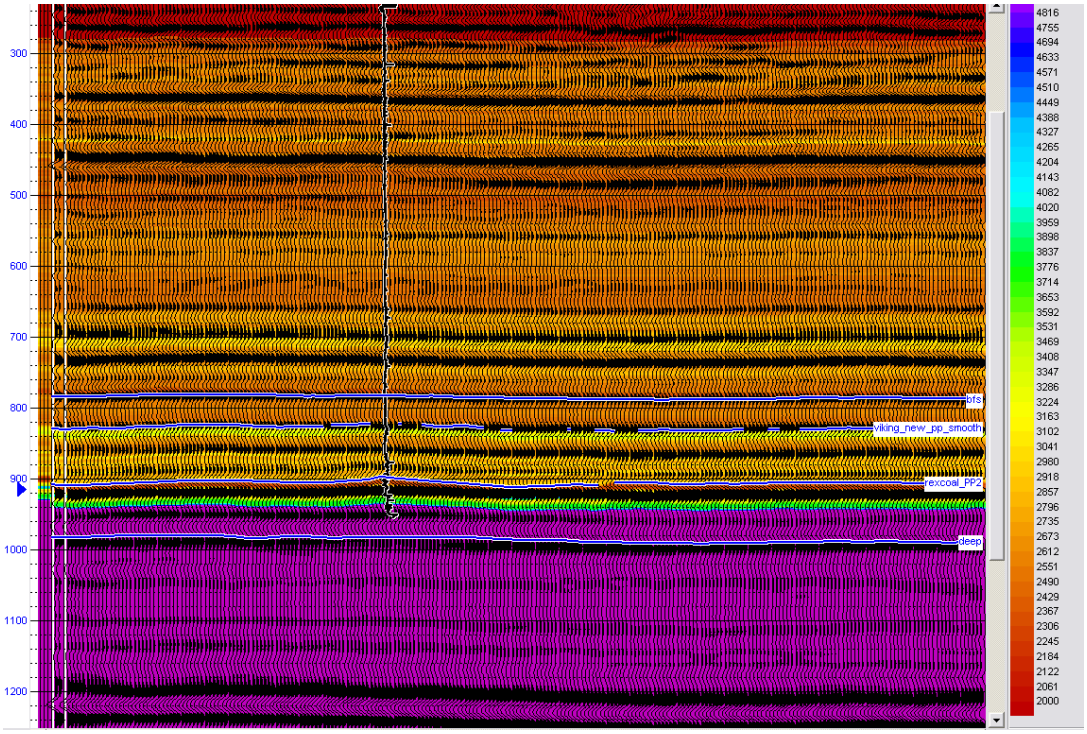

FIG. 15: P-wave velocity from background model used for prestack inversion and the joint prestack inversion.

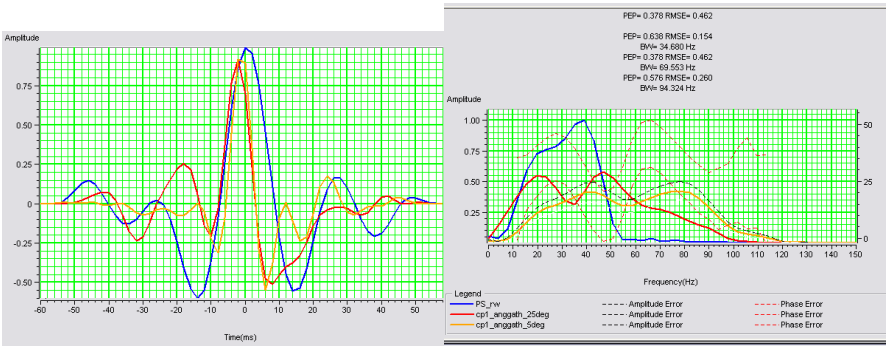

FIG. 16: Near (blue) and far (red) angle wavelets from P-wave data compared to the converted wave wavelet used in joint prestack inversion. Note that the converted wave wavelet is significantly lower bandwidth than either P-wave wavelet. The average phase on the converted wave wavelet is -7°.

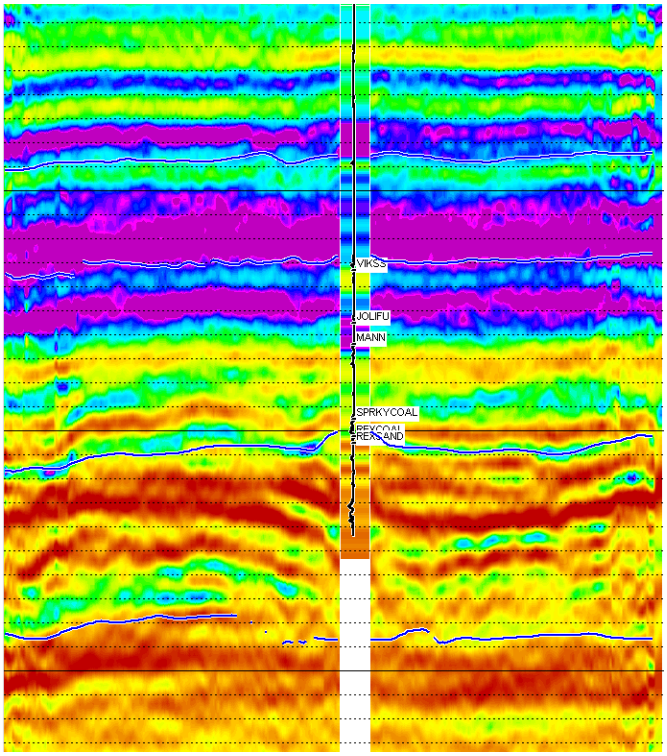

FIG. 17: Vp/Vs from joint prestack inversion. Vp/Vs from logs at Well D has been inserted in colour and the SP log as the trace.

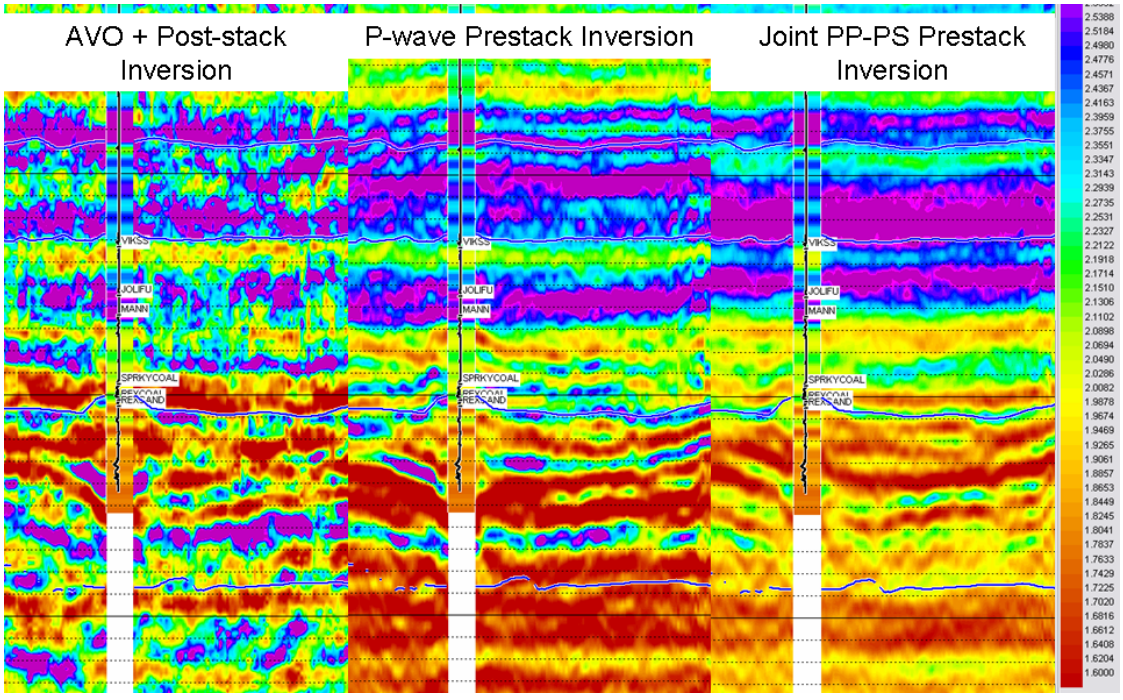

FIG. 18: Comparison of Vp/Vs calculated from AVO + post-stack inversion (left), prestack inversion (middle) and joint prestack inversion (right). Vp/Vs from logs at Well D has been inserted in colour and the SP log as the trace.

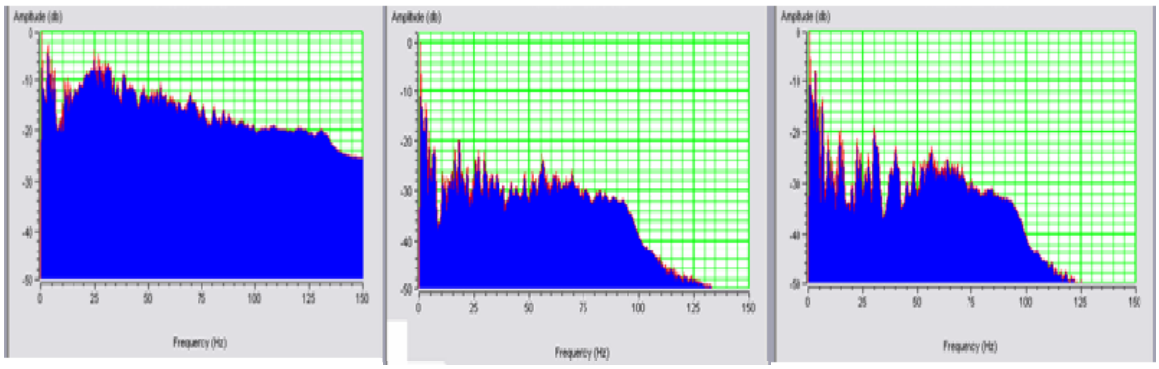

FIG. 19: Amplitude spectra of the Vp/Vs volumes taken from 10 inlines around well F. The left image shows the amplitude spectrum from the AVO + post-stack inversion has significantly more high frequency energy than either, the prestack inversion (middle) or the joint prestack inversion (right).

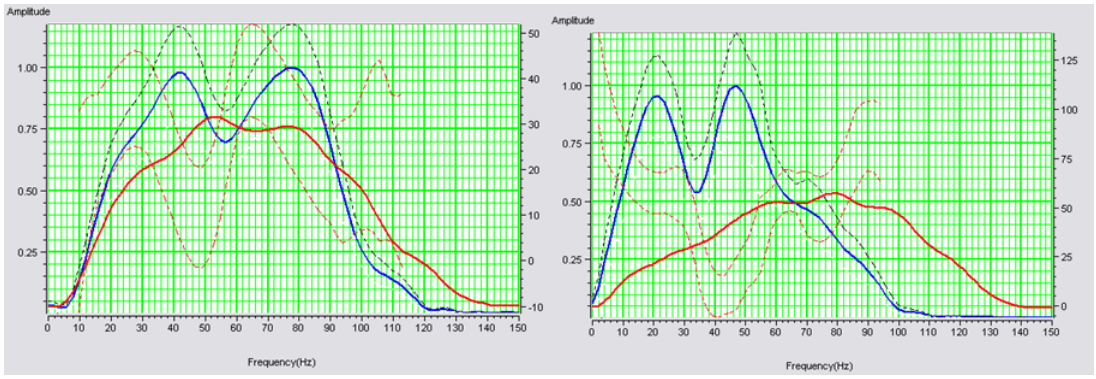

FIG. 20: Amplitude spectra of the wavelet used in the inversions. The left image shows a comparison of the near angle wavelet (blue) with the wavelet used to invert the P-wave reflectivity (red). A similar comparison is shown for the far angle (blue) and the S-reflectivity wavelet (red).

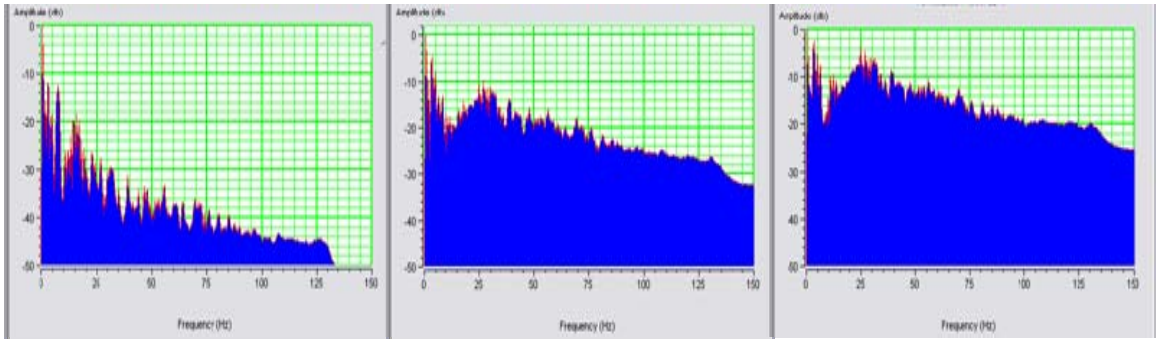

FIG. 21: Amplitude spectra of the attributes derived from the AVO + post-stack inversion flow. The left image shows the spectrum from the P-Impedance, the middle from the S-Impedance, and the spectrum from the Vp/Vs is on the right. Taking the ratio of the impedances has magnified the enhanced frequency content of the data, possibly by introducing noise.

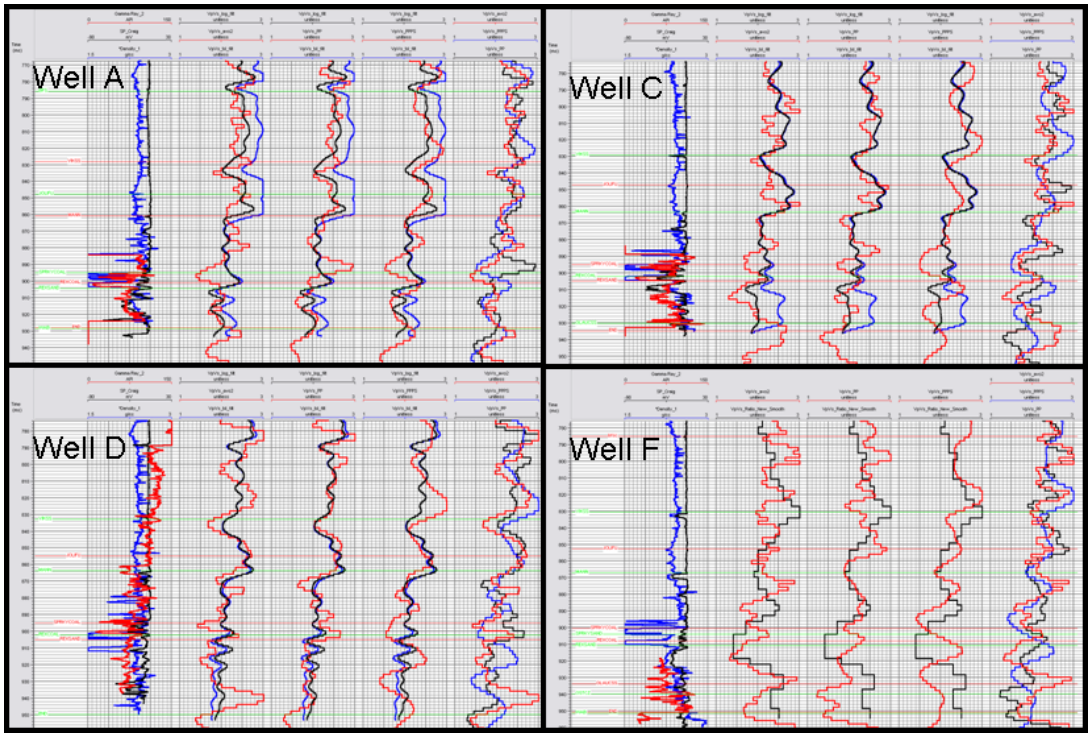

FIG. 22: Detailed trace comparisons for Vp/Vs extracted using on of the three methods discussed above for four wells. The left track shows the Gama Ray (red) SP (black) and Density (blue) logs from the wells where the remaining tracks are comparisons to the various inversions in the order in which they were completed, AVO+post stack, prestack, joint prestack (black=log Vp/Vs, red=inversion, blue=depth-time). The 5th track compares each method directly.

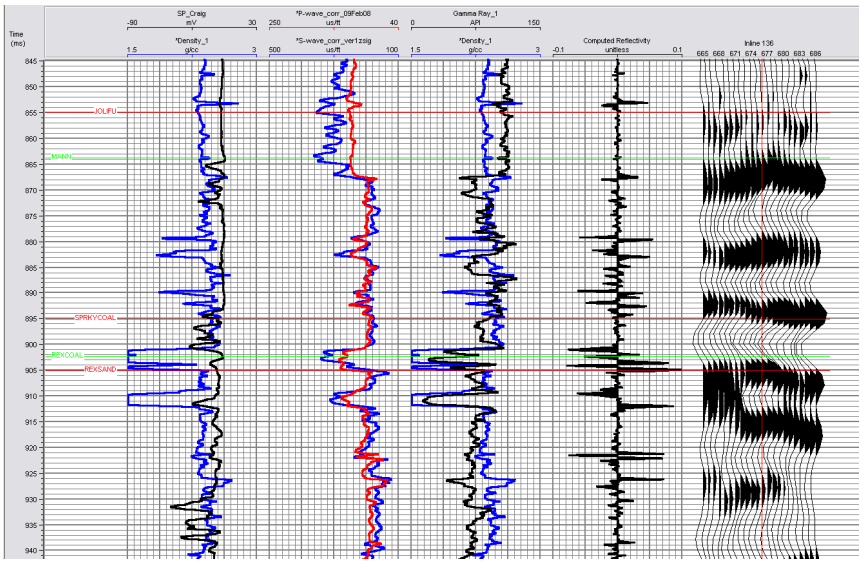

FIG. 23: Plot of well logs for well D. Reflectivity is plotted in the 4th track and shows that the small reflectivity assumption is violated by the coals.